Water Research 256 (2024) 121625

Contents lists available at ScienceDirect

Water Research

journal homepage: www.elsevier.com/locate/watres

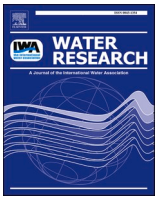

Enhanced bioelectroremediation of heavy metal contaminated groundwater through advancing a self-standing cathode

Jafar Ali [a,b], Changhong Zheng [a,b], Tao Lyu [c,*], Nurudeen Abiola Oladoja [d], Ying Lu [a,b], Wengang An [a,b], Yuesuo Yang [a,b,*]

[a] Key Lab of Groundwater Resources and Environment (Jilin University), Ministry of Education, Changchun 130021, China
[b] Jilin Provincial Key Laboratory of Water Resources and Environment, Jilin University, Changchun 130021, China
[c] School of Water, Energy and Environment, Cranfield University, College Road, Bedfordshire MK43 0AL, UK
[d] Hydrochemistry Research Laboratory, Department of Chemical Sciences, Adekunle Ajasin University, Akungba Akoko, Nigeria

ARTICLE INFO

Keywords:
Bioelectricity
Carbon nanofibers
Chromium
Electroremediation
Green technologies
Toxic metals

ABSTRACT

Hexavalent chromium (Cr(VI)) contamination in groundwater poses a substantial global challenge due to its high toxicity and extensive industrial applications. While the bioelectroremediation of Cr(VI) has attracted huge attention for its eco-friendly attributes, its practical application remains constrained by the hydrogeochemical conditions of groundwater (mainly pH), low electron transfer efficiency, limitations in electrocatalyst synthesis and electrode fabrication. In this study, we developed and investigated the use of N, S co-doped carbon nanofibers (CNFs) integrated on a graphite felt (GF) as a self-standing cathode (NS/CNF-GF) for the comprehensive reduction of Cr(VI) from real contaminated groundwater. The binder free cathode, prepared through electropolymerization, was employed in a dual-chamber microbial fuel cell (MFC) for the treatment of Cr (VI)-laden real groundwater (40 mg/L) with a pH of 7.4. The electrochemical characterization of the prepared cathode revealed a distinct electroactive surface area, more wettability, facilitating enhanced adsorption and rapid electron transfer, resulting in a commendable Cr(VI) reduction rate of 0.83 mg/L/h. The MFC equipped with NS/CNF-GF demonstrated the lowest charge transfer resistance (R_{ct}) and generated the highest power density (155 ± 0.3 mW/m^2) compared to control systems. The favorable electrokinetics for modified cathode led to swift substrate consumption in the anode, releasing more electrons and protons, thereby accelerating Cr(VI) reduction to achieve the highest cathodic coulombic efficiency ($C.E_{ca)\ of}$80 ± 1.3 %. A similar temporal trend observed between Cr(VI) removal efficiency, COD removal efficiency, and $C.E_{ca,}$ underscores the effective performance of the modified electrode. The reusability of the binder free cathode, exemption from catholyte preparation and the absence of pH regulation requirements highlighted the potential scalability and applicability of our findings on a larger scale.

1. Introduction

Chromium (Cr) stands as a prevalent heavy metal extensively used in various industries, including electroplating, stainless steel, metallurgy, leather, and dyeing (Dang et al., 2023; Xu et al., 2023). However, Cr is recognized as a toxic substance, posing serious threats to both living organisms and the environment, particularly when introduced into the food chain (Batayneh, 2012). Consequently, stringent regulations governing the use and discharge of Cr have been implemented worldwide. Despite these regulations, considerable levels of Cr can be found in soil (800 mg/kg) and aquatic environments (120 mg/L) due to inappropriate discharge (Chen et al., 2021a; Zhang et al., 2023b). Such conditions usually cause further surpass of statutory limits of 0.1 and 0.05 mg L^{-1} for drinking water and surface water, respectively (Ali et al., 2021; Yu et al., 2022). This discrepancy highlights the needs for effective and sustainable strategies to remediate Cr contamination in environmental matrices, necessitating continual research endeavors and dedicated efforts. Various Cr remediation methods, including adsorption, ion exchange, electrochemical, and bioremediation processes, have been developed and deployed (Chen et al., 2021a; Prasad et al., 2021).

Among these, the synergetic bioelectrochemical method based on microbial fuel cells (MFCs) has emerged as a promising choice, attributed to its unique benefits of ambient working conditions, renewable energy generation, and the absence of sludge production (Ali et al.,

* Corresponding authors.
E-mail addresses: t.lyu@cranfield.ac.uk (T. Lyu), yangyuesuo@jlu.edu.cn (Y. Yang).

https://doi.org/10.1016/j.watres.2024.121625
Received 11 January 2024; Received in revised form 13 April 2024; Accepted 15 April 2024
Available online 15 April 2024

2020b). The anaerobic oxidation of organic matter liberates electrons and protons, which can be delivered from bioanode to the cathode. The highly toxic and mobile Cr(VI) act as the terminal electron acceptor and get reduced to less toxic and mobile Cr(III), thereby achieving Cr remediation (Song et al., 2022; Xafenias et al., 2013). Continues efforts within MFCs have been dedicated to optimizing performance, with a primary focus on reducing the overpotential of cathodes. This involves strategies such as enriching electroactive bacteria and manufacturing electrodes with metal oxide nanoparticles and conductive nanomaterials (Fu et al., 2021). Notably, the use of abiotic cathodes based on graphene, multiwalled carbon nanotubes (MWCNT), or carbon nanofibers (CNFs), with minimal metals modifications (e.g., Fe, Cu, Al, Ni), has been deemed to significantly increase the conductance and electrokinetic of electrodes. This approach holds the potential to improve contaminant remediation performances of MFCs (Hidayat et al., 2022; Li and Zhou, 2018). In the context of Cr remediation, a series of exploration into MFC technology has emerged over the past decade. Noteworthy contributions include the utilization of a graphite cathode, which reported a substantial power density of 150 mW/m^2 coupled with a Cr(VI) reduction rate of 0.67 mg/L/h (Wang et al., 2008b).

Advancements in cathode performance have been achieved through the incorporation CNFs, resulting in significantly elevated power density and Cr(VI) reduction rate at 970 mW/m^2 and 0.7767 mg/L/h respectively (Zhang et al., 2012). Explorations involving mediator metals, e.g., Fe (III) and Cu (II), demonstrated enhanced transformation of different valence states of Cr. For instance, use of FeS@rGO cathode dramatically boosted the Cr(VI) reduction rate to 1.43 mg/L/h (Ali et al., 2020a). Despite the significant developments facilitated by these modification procedures, a critical challenge remains in the form of powder-based electrocatalyst, which needs binders to be applied on the electrode surface. This approach results in higher cost, low resilient performance, and the potential risk of metal leaching as secondary pollution (Fan et al., 2023). Furthermore, most investigations have been confined to synthetic contaminated water conditions, lacking robust evidence to support real-world applications. An optimal cathode should be easily preparable, generate no secondary pollution, exhibit fast electrokinetics, and operate effectively under natural environmental conditions. In this regard, binder-free cathodes prepared via in situ polymerization, possessing enhanced electrochemical properties can fulfill the prerequisites for efficient bioelectroremediation of Cr(VI) in real contaminated water (Li and Zhou, 2018; 2019; Wang et al., 2008a; Wu et al., 2019).

Notably, polyaniline (PANI)-based binder-free electrodes have been developed for electric energy conversion due to their excellent conductivity and facile synthesis by polymerization (Luo et al., 2022; Zhang et al., 2021). Although attempts have been made to enhance Cr(VI) reduction in photochemical fuel cells (Fan et al., 2023; Li and Zhou, 2018) using metal dopped carbon materials, but metal leaching remains a concern, potentially leading to secondary pollution and reduced effectiveness. Meanwhile, metal free carbon nanofibers (CNFs) have displayed remarkable electrocatalytic properties credited to turbostratic structure of carbon (Walters et al., 2014; Xu et al., 2018). Given the exceptional adsorption and reduction capabilities of Cr(VI) exhibited by N and S doped carbon nanomaterials, attributed to increased interaction by Van der Waals force, in situ reduction, electrostatic interaction and chemical complexation (Chen et al., 2022; Zhou et al., 2022), Thus, it is hypothesized that N, S co-doped CNFs on graphite felt (NS/CNF-GF) can serve as a self-standing cathode for rapid Cr(VI) reduction, overcoming challenges associated with metal leaching and operational pH barriers. Conductive network of CNFs possessing numerous active sites can enhance the hydrophilicity of cathodes, adsorption, electrokinetics, and removal of Cr(VI) from real contaminated water.

To the best of our knowledge, use of binder free cathodes for treating Cr(VI) contaminated real groundwater is not well reported. This study aims to prepare and demonstrate the self-standing cathode for the removal of Cr in real contaminated groundwater samples (40 mg/L and pH 7.4) collected from an abandoned industrial site. The method presented obviates that need for catholyte preparation, catalyst binders, and pH regulation for Cr(VI) reduction. The results of this study will contribute valuable insights supporting the practical applications of an in situ synthesized electrode with enhanced electrokinetics, facilitating sustainable remediation of heavy metal-contaminated groundwater.

2. Materials and methods

2.1. Study area, groundwater sampling and analysis

The study area is a legacy site of a Cr chemical plant situated in the northwest region of Xinxiang city, Henan province, China. Xinxiang city is located at the southeastern base of the Taihang mountains and the northern edge of the alluvial plain in the middle reaches of the Yellow River. The surface composition of the study area exhibits a quaternary river-phase sedimentary layer with a thickness of 50–60 m, primarily comprised of clay and sand lithology. The primary processes contributing to aquifer recharge include atmospheric precipitation, irrigation recharge, and lateral runoff. Shallow groundwater (depth < 30 m) is mainly hosted in the quaternary aquifer, while deep groundwater (depth > 30 m) is typically found in the Cretaceous aquifer. The study site covers an area of 4666 m^2 and has been used for the deposition of Cr slag by a chromate production plant established in 1993. Inadequate anti-seepage measures during the stacking of Cr slag have led to the seepage of contaminates, affecting both soil and groundwater. Despite the closure of the Cr chemical plant in 1995, the average Cr concentration in the topsoil has reached 12,100 mg/kg. Recent hydrogeochemical analyses and numerical modeling of this contaminated site have revealed the presence of Cr(VI) contamination and its migration into the deep groundwater (Chen et al., 2021a; Zhang et al., 2023b).

Eight groundwater samples were collected from the Cr slag stacking plot within the study area (Fig. 1a). Samples were divided into low Cr (VI) group (LCG) and high Cr(VI) group (HCG) having 7.8–40 and 51–280 mg/L respectively, based on the groundwater quality standards specified in China (GB/T 14,848–2017). Before sampling, groundwater was pumped out at the rate of 100 mL/min using submersible pump until water quality parameters (i.e., dissolved oxygen (DO), pH, and oxidation–reduction potential (ORP) were stable. Groundwater samples were collected in 5 L brown glass bottles, which were washed with deionized water before sampling. The water samples were sent to the laboratory within 8 h after collection and stored in a 4 °C refrigerator for further testing. Water quality parameters, such as DO, pH, ORP were immediately analyzed using portable device (DZB-718, INESA, China) in the field. Other chemical indicators (Cr, Na^+, Ca^{2+}, Mg^{2+}, Mn, Fe, HCO_3^-, SO_4^{2-}, Cl^-, NO_3^-) were measured in Key Laboratory of Groundwater Resources and Environment (Jilin University). The Cr(VI) concentration in the groundwater was determined using diphenylcarbazide spectrophotometry method (752 G UV–VIS Spectrophotometer, INESA, China).

2.2. Binder free and self-standing cathode synthesis and chracterization

The NS/CNF-GF cathode was synthesized through a cyclic voltammetry (CV) electrodeposition method. A GF electrode ($4 \times 2.5 \times 0.5$ cm) was immersed in a mixed solution, consisting of equal volumes of 0.2 M aniline and 0.6 M H_2SO_4, for a duration of 24 h. For the electrode fabrication process, CV was executed in a three-electrode system using GF as working electrode, Ag/AgCl and Pt wire as the reference and counter electrodes, respectively. The potential range applied was −0.2 to 1.2 V with a scan rate of 10 mVs^{-1} for 10 cycles. Following the electro-deposition, GF was covered with hierarchical PANI nanofibers, subjected to rinsing with deionized water and ethanol, and subsequently dried at 60 °C (Fig. 1b). To obtain the CNF-GF, the initial step involved pyrolysis at 550 °C for 2 h, with a temperature ramp rate of 5 °C min^{-1} in a nitrogen atmosphere. For N, S co doping, CNF-GF electrodes were dipped in a 0.25 M thiourea solution for 8 h, followed by a second

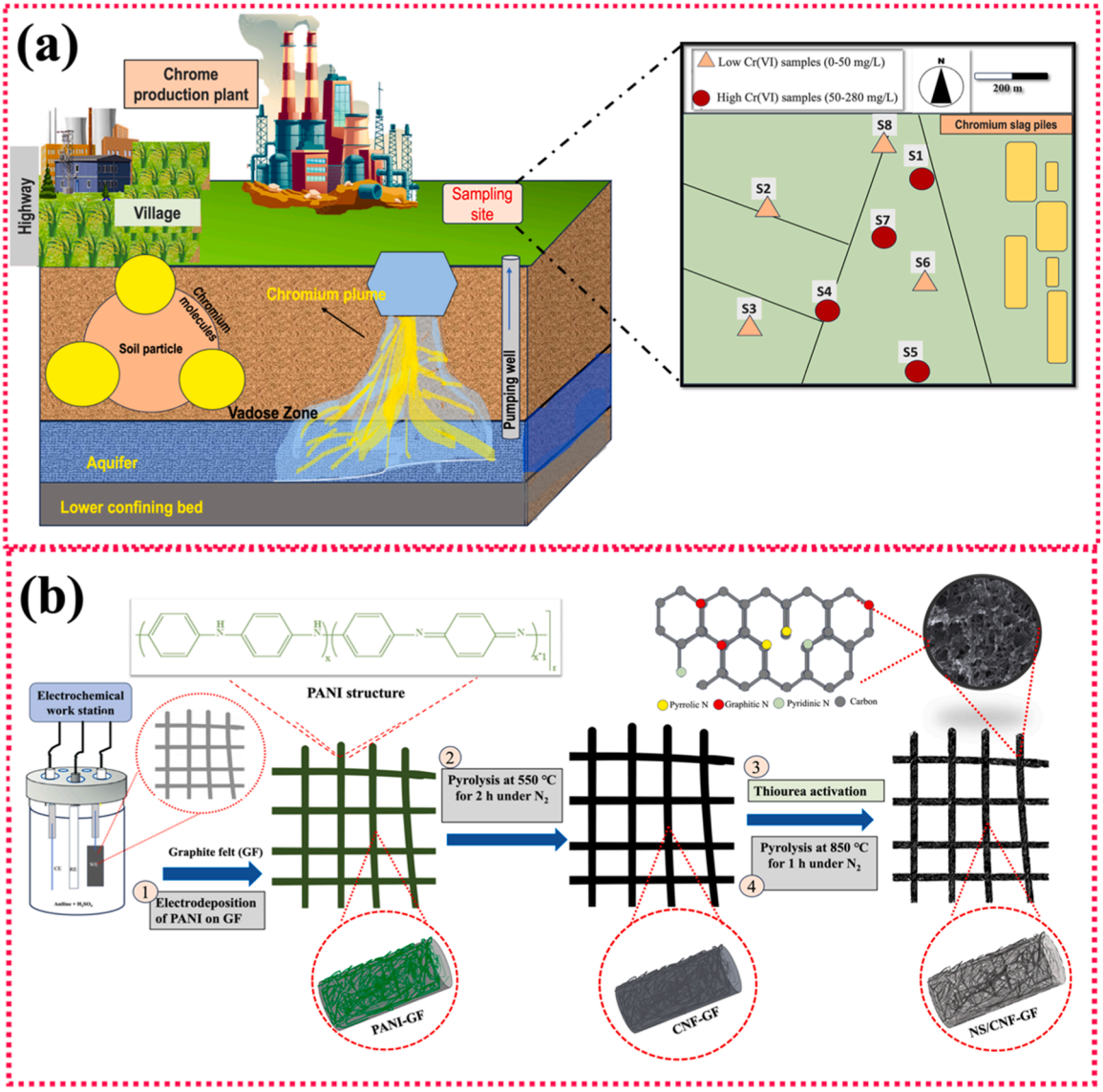

Fig. 1. (a) Description of the study area indicating the location of slag piles and sampling points, (b) **s**chematic illustration of synthesis process for binder free electrode (NS/CNF-GF).

pyrolysis at 850 °C for 1.5 h (Chen et al., 2020). CNF-GF and GF, without thiourea treatment or any form of modification, were processed as control specimens. The surface morphology, chemical composition, and structure of the in situ synthesized electrodes were determined by scanning electron microscope (SEM, Apreo S), energy dispersive spectrometer (EDS, X-Max20), and A Tecnai G2 TF20 transmission electron microscope (TEM, FEI, USA) operating at 300 KV. The hydrophilicity/wettability of the electrodes was examined by a contact angle (Dataphysics OCA 50) instrument. Further insights into the detailed chemical composition and structural bonding of the modified electrodes were obtained using X-ray photoelectron spectrometer (Thermo Scientific Escalab 250Xi). The chemical structure of the modified electrodes was further verified by X-ray diffraction (XRD) analysis performed with a Bruker D8A X-ray diffractometer using Cu-Kα radiation (tube voltage: 40 kV; current: 40 mA; scan angle 2θ range: 10–80°; scan rate: 5°/min).

2.3. Electrolyte preparation, MFC construction and operation

Three types of dual chamber MFCs were made of plexiglass and each chamber had an effective working volume of 130 ml. Carbon fiber brush (3.5 cm long and 2.5 cm in diameter), purchased from Shanghai Hesen Electrical Co., Ltd. was used as anode following a pretreatment procedure. This involved a 24 h incubation in an acetone solution, followed by heating in a muffle furnace at 450 °C for 30 min (Ali et al., 2019). A proton exchange membrane (PEM, NafionTM 117, Dupont Co.), with an active surface area of 12.56 cm^2 was used as separator between both chambers. For the activation process, PEM was boiled in H_2O_4 (30 % v/v in deionized water) and 0.5 M H_2SO_4, each for 1 hour and then kept in deionized water. Groundwater collected from the Cr contaminated site (samples with 40 mg/L of Cr(VI) and pH of 7.4) was directly used as catholyte. The anolyte was prepared by dissolving the following compounds (g/L) in distilled water: 2 $C_2H_3NaO_2$, 4.4 KH_2PO_4, 3.4 K_2HPO_4, 1.0 KNO_3, 0.5 NaCl, 0.2 $MgSO_4$, and 0.014 $CaCl_2$. Additionally, 1 mL from trace elements media containing the following (mg/L) was added: 0.39 $Na_2MoO_4{\cdot}2H_2O$, 0.22 $ZnSO_4{\cdot}7H_2O$, 1.81 $MnCl_2{\cdot}4H_2O$, 0.08 $CuSO_4{\cdot}5H_2O$, and 2.86 H_3BO_3. All MFCs were assembled and were named according to the type of cathode i.e., MFC with NS/CNF/GF, CNF/GF, and GF designated as MFC-A, MFC-B, and MFC—C, respectively. Each type of MFC was run in triplicate (total 9) to ensure the reproducibility of the study. Nitrogen purging was employed to remove the DO from the electrolytes. Sewage sludge was used as source of anodic inoculum. All MFCs were incubated at room temperature and

allowed to run in open circuit (OC) mode. Once, stabilized open circuit potential (OCP) was achieved, the MFCs were ready for electrochemical analysis. A copper wire (0.15 mm) connected both electrodes through an external resistance, and the potential was recorded at 15 min interval by a digital multimeter data acquisition system (M2700, Keithley instrument, Cleveland, USA).

2.4. Electrochemical performance and calculations

The electrochemical characterization of the modified electrodes was conducted using electrochemical impedance spectroscopy (EIS) and cyclic voltammetry (CV) with the CHI660E electrochemical workstation system (CH Instruments, Inc.) in a three-electrode system. In all measurements, the cathode served as the working electrode, while the anode and Ag/AgCl were employed as counter and reference electrodes, respectively. For EIS analysis, closed circuit MFCs were subjected to a frequency range from 100 kHz to 10 mHz with an AC signal of 10 mV amplitude at the OCP of the cathode. The Nyquist plot obtained from EIS facilitated the estimation of electrolyte resistance, charge transfer resistance (R_{ct}), and diffusion resistance (W). Later, Z view software was used to fit the electrochemical impendence spectra to the equivalent circuit. The electrochemical reduction of Cr(VI) on the cathode was investigated using CV in a unit cell, with the electrolyte prepared by mixing equal volume of Cr(VI) contaminated groundwater and 0.1 M H_2SO_4. A Pt wire served as the counter electrode, maintaining the same electrode connections as mentioned in the EIS. For CV analysis, the potential was scanned from −1.2 to 1.2 V at a scan rate of 10 mv/S. For further electrochemical chracterization of MFCs, polarization curves were drawn by changing external resistance from high to low and measuring the cell potential. Current and power densities were calculated from potential data using Ohm's law (V=IR_{ext}), normalized with the exposed cathode surface area. The Cr(VI) removal performance of MFCs was investigated in OC and CC using fed batch mode for 60 h. The pH and Cr(VI) concentration in catholyte samples were determined using the pH meter (Orion 3-star, Thermo Scientific, USA) and standard 1,5- diphenylcarbazide colorimetric method respectively, as mentioned in a previous study (Ali et al., 2020a). The removal efficiency for Cr(VI) was calculated by Eq. (1), where C_0 and C_t indicate the initial concentration and concentration at specific time respectively.

$$\text{Chromium removal efficiency } (\%) = E_{Rem} = \frac{C_0 - C_t}{C_0} \times 100 \quad (1)$$

Cathodic coulombic efficiency ($C.E_{ca}$) depict the ratio of charges used for Cr(VI) reduction to Cr(III) charges flowing across the external resistance in MFCs (Zhang et al., 2023a). Hence, $C.E_{ca}$ was determined by Eq. (2), Where, is the number of electrons to reduce the Cr(VI), ΔC is the change in concentration during the operation time t, V_{ca} is the volume of cathode chamber, M_{Cr} (52 g/mol) the molecular weight of Cr, F the Faraday's constant (96,485 C/mol), 10^3 the conversion unit (mg/g), I is the circuital current and T is the operation time of MFC.

$$C.E_{ca} = \frac{aF\ \Delta C_{cr(IV)}\ V_{Ca}}{10^3\ M_{Cr} \sum_{i=1}^{n} Ii\Delta ti} \quad (2)$$

2.5. Chromium reduction kinetics

In this study, Cr(VI) reduction kinetics were regressed using the first order equation (Eq. (3)) as follow:

$$C_t = C_0\ e^{-Kt} \quad (3)$$

Which can be linearized by taking the natural logarithm on both sides as:

$$\ln C_t/C_0 = -Kt \quad (4)$$

where k is the first-order rate constant calculated from the slope of ln C_0/C vs. time graph and where C_0 and C represent the initial concentration and concentration at various time intervals t in Eq. (4).

2.6. Statistical analysis

The results were expressed as mean ± standard deviation for each experiment with a triplicate analysis. For statistical analysis one way ANOVA test was performed using IBM SPSS statistics for window version 26.0 (Armonk, NY: IBM Corp), considering P-values less than 0.05 statistically significant.

3. Results and discussion

3.1. Chromium concentration and hydrogeochemical parameters

To investigate the broader feasibility of the proposed modified cathode for Cr(VI) reduction in groundwater, this study involved the collection and analysis of multiple samples to first determine the concentration range of Cr(VI). The collected groundwater samples were categorized into two groups, i.e. LCG and HCG, based on observed Cr (VI) concentration levels ranging from 51 to 280, and 7.8 to 40 mg/L, respectively (Table S1). In this study, groundwater from LCG with an intermediary Cr(VI) concentration of 40 mg/L and a pH of 7.4 was selected to assess the proposed methods. Due to the presence of high carbonates, bicarbonates, and chromium hydroxides, samples from HCG exhibited high alkaline pH values (8–9.2), which are not common pH ranges compared to other Cr contaminated waters. Therefore, the current effort did not focus on these water samples and further studies for these samples will be conducted based on the evidence collected in this study.

3.2. Chracterization of self-standing cathode (NS/CNF-GF)

The original GF had a smooth surface before the electro polymerization of aniline (Fig. 2a). After in situ polymerization, a conductive network of interconnected PANI nanofibers was evolved on the GF surface (Fig. 2b-c). During the annealing process, simultaneous carbonization of PANI nanofibers and decomposition of thiourea integrated the in-situ etching of CNFs. The previous study reported that a reducing activation atmosphere can be created from in situ generated gases i.e., NH_3, H_2S, and CS_2 by degradation of dip coated thiourea (Chen et al., 2020). The adsorption of activation gasses in macro and mesopores of CNFs could generate turbostratic domains from PANI precursors during thiourea activation, to improve the electroactive surface area of the electrode material for high mass transfer. Briefly, small micropores and turbostratic regions were created on CNFs after strong thiourea etching, while carbonization shrunken the CNFs to further reduce their diameter and widened the macropores. The carbon fiber structure was maintained after infiltration of thiourea, and carbonization resulted in more dense agglomeration of CNFs (Fig. 2e). Hence more crosslinking of conductive CNFs will reduce the charge transfer resistance for cathodes.

Noticeably, thiourea not only worked as N, S-containing precursor molecule but also activated the CNFs structure for pore generation and modification (Chen et al., 2020; Qiu et al., 2019). More structural details of cathodes were observed by TEM analysis and results are presented in Fig. 2h-i. The crosslinked and interconnected structure of conductive CNFs was retained during harsh carbonization and sample preparation steps for TEM analysis. Moreover, turbostratic carbon domains can be clearly seen from HRTEM image (Fig. 2i), which indicate thiourea etching resulted in randomized stacking of graphite layers on CNFs. The turbostratic carbon structure is a unique class of carbon, ordering between amorphous phase and crystalline graphite phase and have exceptional electrocatalytic features (Jalalabadi et al., 2023; Lai et al., 2020). Stability of CNFs over GF surface can be ascribed to the covalent bond between carbon atoms, which devoid the use of binder for

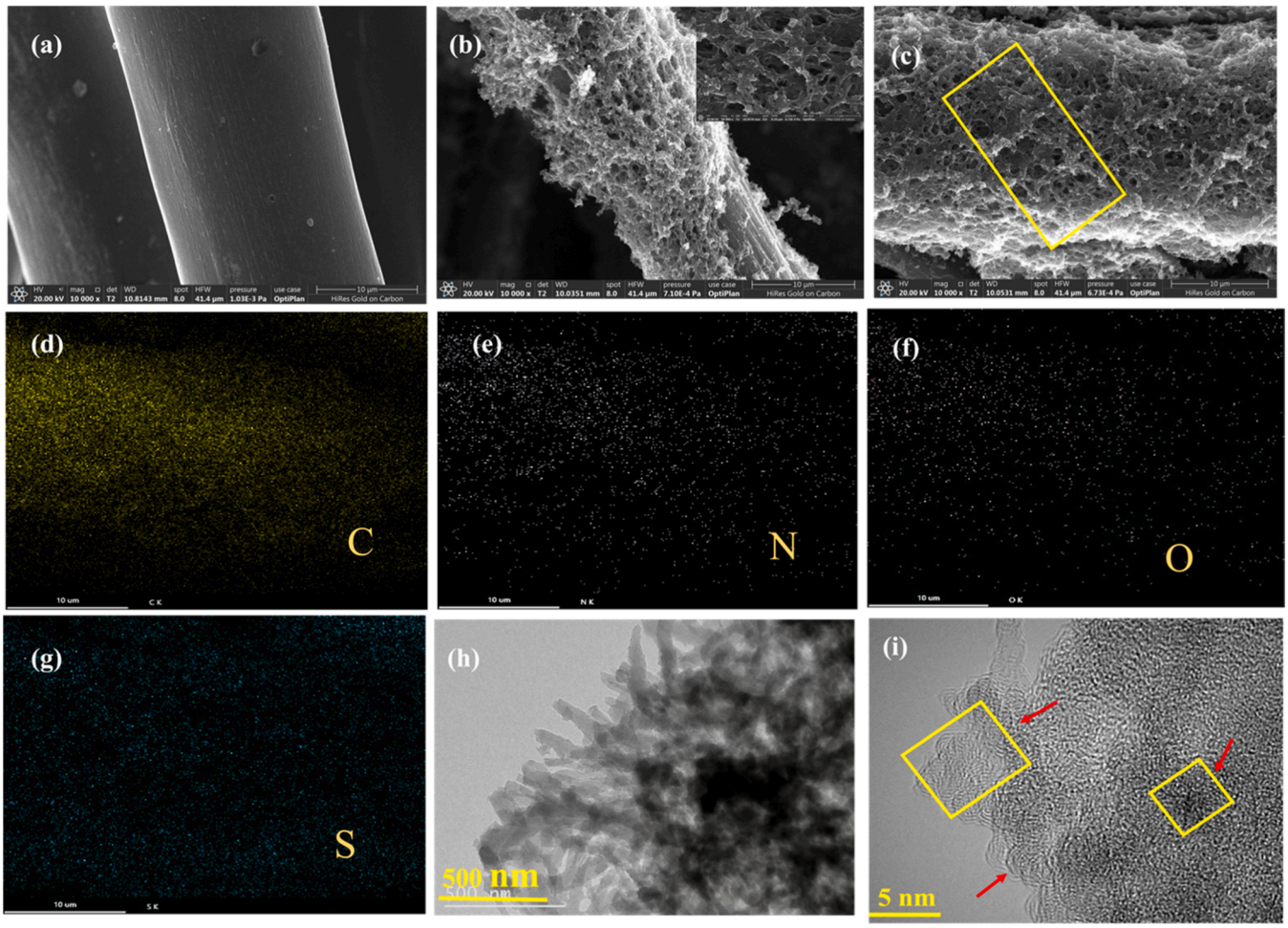

Fig. 2. SEM image of plain GF (a), CNFs on GF (b), NS/CNF-GF (c), elemental mapping of NS/CNF-GF(d-g), TEM images of NS/CNF-GF(h-i).

electrode fabrication. Overall NS/CNF-GF has the compact and rougher surface due to strong etching of thiourea (Liu et al., 2017). Energy dispersive spectrometer (EDS) measurement showed the homogenous distribution of C, O, N, and S element (Fig. 2d-g). The dopant N and S are believed to be originated from aniline (amine group) and thiourea respectively (Qiu et al., 2019). Graphitic N improves the electron transfer, while pyridinic and pyrrolic N promote the electron donor effect using lone pairs and conjugate with carbon framework Partial graphitization is believed to facilitate the introduction of N containing active sites on CNFs (Li et al., 2020; Xu et al., 2016). The S doping increased the wettability of modified electrodes, as confirmed by contact angle of NS/CNF-GF (56–57°) indicating the high hydrophilicity compared with control electrodes (Fig. S1). Improved hydrophilicity of cathodes represent their potential to improve the mass transfer kinetics for pollutants in water purification (Mohapatra et al., 2019).

Surface chemistry of electrode plays crucial role in electrocatalytic reactions, which was tuned by thiourea activation in this study. The XPS results showed obvious peaks of C, N, O, and S confirming the dual doping of CNFs surface with N and S (Fig. 3a). The high-resolution C1s spectrum was resolved into 4 individual peaks corresponding to the C-C, C=C (~ 283 eV), C-N (~286.2 eV), C=O (~287 eV), and COOR (~ 289 eV) bindings (Fig. 3b). Presence of two small peaks at 286.2 eV and 289 eV reflect different bonding structure of C—N bonds, which can be further assigned to N-sp^2 C and N-sp^3 C bonds respectively, signifying the substitution of N atoms to the defects of CNFs after reacting with thiourea (Chen et al., 2014). The binding energy of 286 eV has been designated to sp^3 hybridization of turbostratic carbon based membranes (Wollbrink et al., 2016). Three typical peaks appeared at 398.2 eV (–*N*=), 400.4 eV (–NH^+=) and 401.75 eV (–NH_2^+–), validating the successful in situ synthesis of CNFs over GF(Fig. 3c). The N 1 s spectrum contain three types of N, such as graphitic N (~401 eV), pyridinic (~398 eV) and pyrrolic N (~400 eV) which typically appear in N dopped carbon nanomaterials (Wu et al., 2019), hence validating the successful synthesis of self-standing NS/CNF-GF cathode.

A positive interplay between pyridinic and pyrrolic N sites play crucial role in electrocatalytic reduction of environmental pollutants (Shang et al., 2022). Meanwhile, peaks around the 163.3 and 164.8 eV are assigned to S $2p_{3/2}$ and $2p_{1/2}$ of the C−S−C covalent bond, and the peak concentrated at 168.5 eV belongs to C−So_x−C as well (Fig. 3d). The S doped sites promoted the wettability of electrode surface for chemisorption of Cr(VI) and synergistically enhance the electron transfer for electroremediation (Fig. S1). These findings reveal that N, S were co-doped on CNFs and surface chemistry was tuned to generate polarizing electron pairs, creating active sites for improved electrochemical performance of synthesized electrode. The XRD analysis further confirmed the crystallinity and composition of the CNF and N, S-CNF samples. As shown in Fig. 3e, NS/CNF-GF exhibited two broad diffraction peaks centered at around 23° and 44°, which are indicative of the turbostratic microstructure assigned to the (002) and (10) planes of CNFs. Previously, turbostratic carbon nanostructures have been correlated with enhanced conductivity of electrical devices (Jang et al., 2022; Walters et al., 2014; Wei et al., 2022). So, mechanical strength and conductivity of turbostratic domains in CNFs will facilitate Cr(VI) remediation function of self-standing electrode in harsh environmental conditions (Jang et al., 2022; Wei et al., 2022). Overall, structural analysis and morphological chracterization results agreed for the

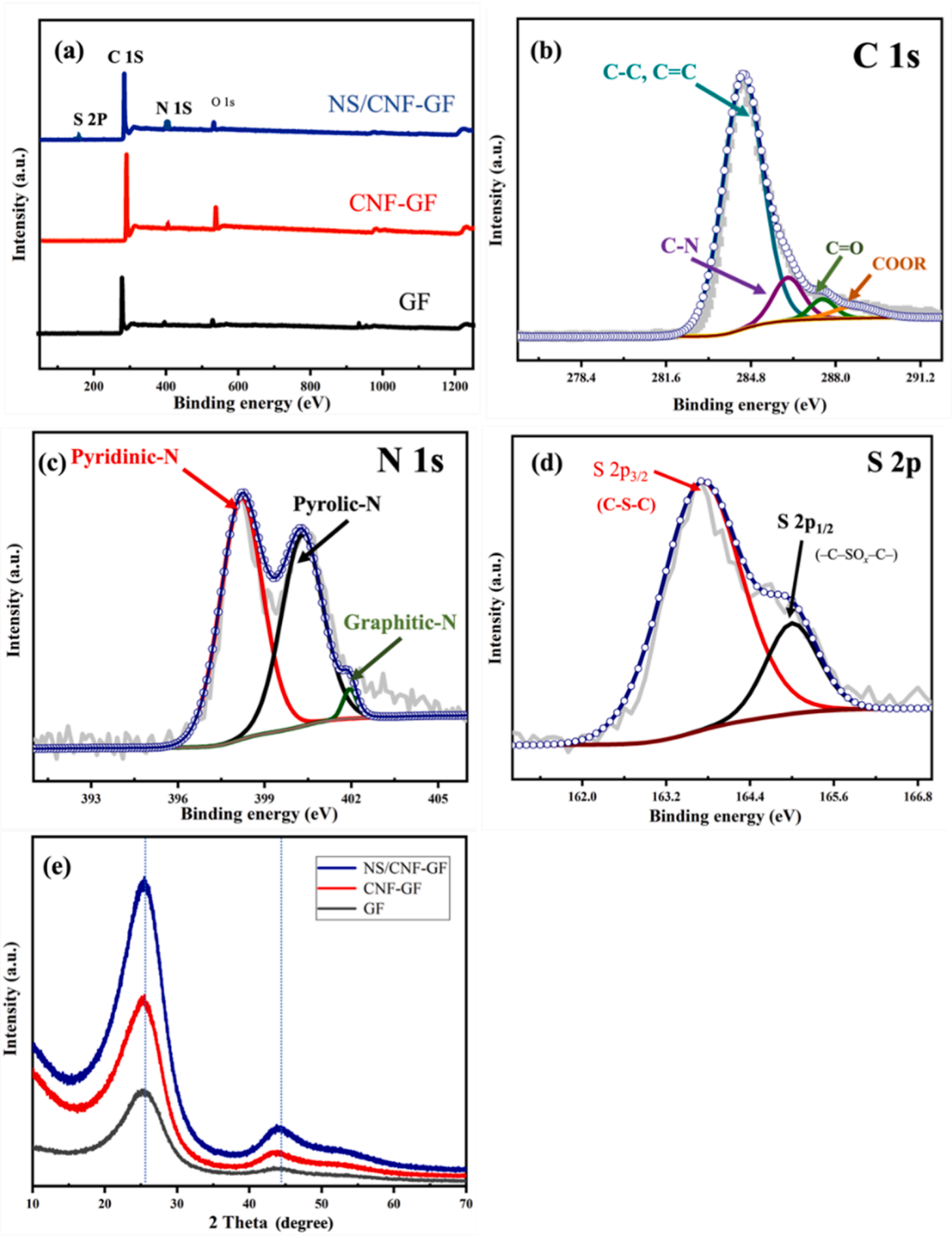

Fig. 3. XPS survey spectra of NS/CNF-GF, CNF-GF, GF(a), high resolution spectra of C 1 s (b), N1s (c), S 2p (d), XRD pattern of all electrodes.

synthesis of stable, electroactive, and resilient NS/CNF-GF electrode.

3.3. Electrochemical performance for Cr (VI) contaminated groundwater treatment

The CV analysis was conducted to investigate the Cr(VI) reduction performance on the surface of modified and control electrodes. All cathodes showed clear Cr(VI) reduction peaks except the blank (Fig. 4a). Small reduction peaks for GF indicated the slow Cr(VI) reduction due to less electroactive surface area and hydrophobic structure (Fig. S1). However, wide reduction peaks were observed for modified electrodes, clearly exhibiting the high potential of modified electrode for prompt Cr (VI) reduction in groundwater samples. Remarkably, the reduction peak for NS/CNF-GF (−0.43 V) were more positive than that of CNF(−0.57 V) and GF(−0.83 V), corroborating that N, S dual doping of CNFs has reduced the over potential, via increased wettability, electron transfer and mass transfer of contaminates. These findings are in accordance with previous reports regarding the electrochemical reduction of Cr(VI)

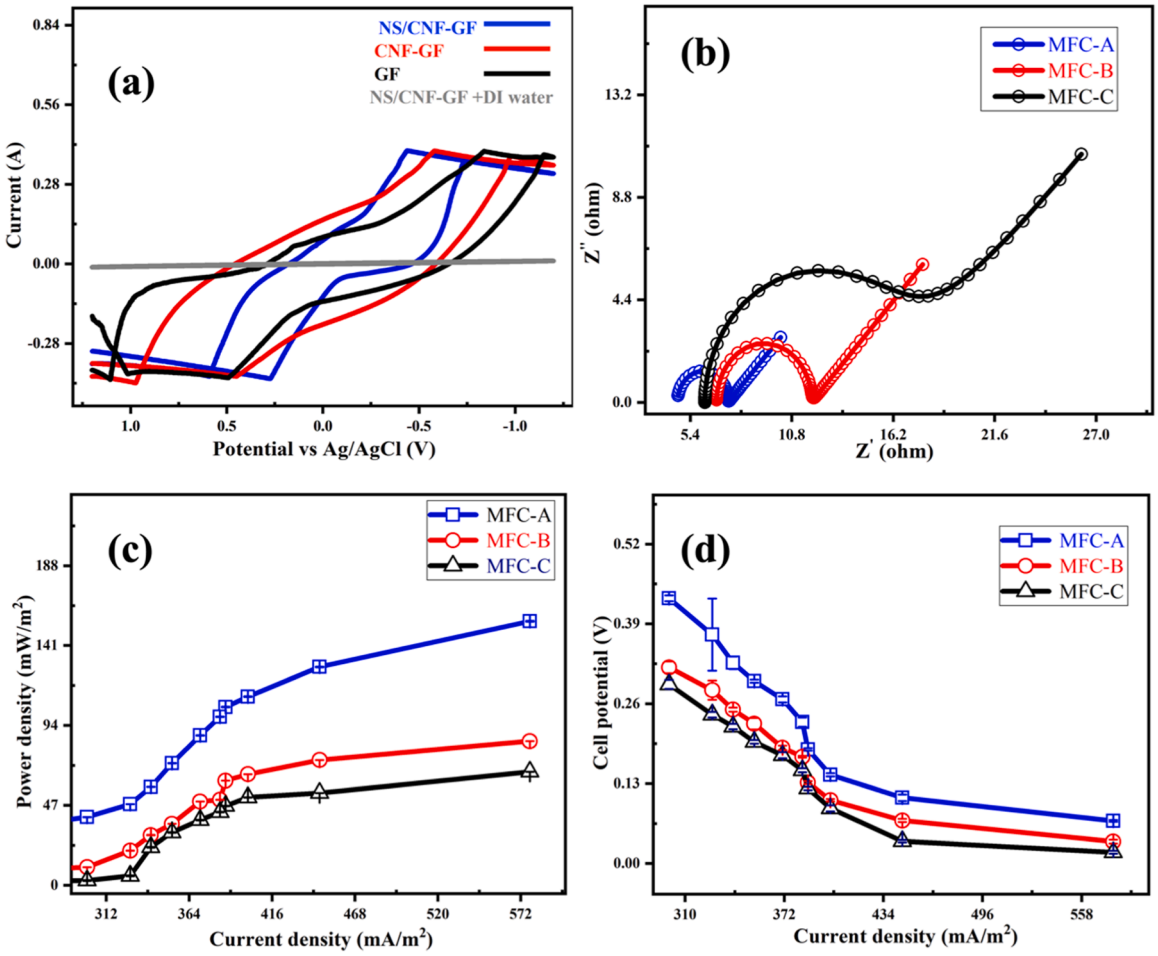

Fig. 4. Cyclic voltammograms for all electrodes in acidic solution (a), EIS analysis (b), Power density and potential (c-d) of MFCs inoculated with Cr (VI) contaminated groundwater.

to Cr (III) in wastewater (Li and Zhou, 2018). A positive shift in the reduction peak for Cr(VI) was observed for CNF-GF and NS/CNF-GF, which can be linked with conductive CNFs and N, S co-doped active sites of modified electrodes respectively. Overall, enhanced Cr(VI) reduction from groundwater can be attributed to chemisorption, complexation and adsorption on modified cathode (Chen et al., 2022). Similarly, reduction current was significantly higher for NS/CNF-GF ($1.08e^{-1}$A) compared with that of CNF ($2.16e^{-2}$A) and GF ($2.5e^{-2}$A), displaying the suitability of in situ fabricated electrode for accelerated Cr(VI) reduction in groundwater (Song et al., 2022).

Further electrochemical conductivity of electrodes was analyzed through Nyquist plots of EIS data. Generally, EIS results are useful to explore total internal resistance and voltage losses during MFCs operation. Overall internal resistance of MFCs can be divided into ohmic resistance (R_{ohm}), charge transfer (R_{CT}) and Warburg mass transfer or diffusion resistance (W). The ohmic resistance (R_{ohm}) indicate the electrolyte or solution resistance and was estimated from first intercept of semicircle in Nyquist plots within the high frequency region. However, diameter of semicircle represents the charge transfer (R_{CT}) on electrode surface, which could be assigned to the electrode conductivity, wettability and processes occurring at electrode-electrolyte interface. The arm of the Nyquist plots specifies the diffusion resistance due low mass transfer in electrocatalytic reduction of Cr (VI). One-time constant model (OTCM) was used to determine all above parameters and data is presented in Table 1. The EIS, results indicate that NS/CNF-GF has notably low ohmic resistance (4.7 Ω) compared with CNF (6.7 Ω) and GF electrodes(6.18 Ω), which is mainly related to the charge distribution at electrode-electrolyte interface, electron mobility and electrolyte conductivity (Fig. 4b). Charge transfer resistance (R_{ct}) for NS/CNF-GF was (2.68 Ω) lower than CNF (5.03 Ω) and GF (10 Ω), which is due to significant electron transfer at the electrode-electrolyte interface. Low R_{ct} also referred to low activation energy and electrode wettability, which describe the better Cr(VI) reduction kinetics for contaminated groundwater. The superior conductivity of NS/CNF-GF can be ascribed to numerous active sites generated by heteroatoms doping on conductive network of CNFs. In the past, multiple conductive nanomaterials and precious cathodes have been applied to reduce the interfacial resistance between cathode and catholytes (Song et al., 2023)., while self-standing cathodes can deliver low resistance under ambient conditions. Likewise, diffusion resistance was lowest for NS/CNF-GF that can be linked with improved hydrophilicity for high mass transfer during electrocatalytic reduction of Cr(VI). Although CNF electrode showed less ohmic and R_{ct} than that of GF but thiourea activation really improved the electrochemical features of NS/CNF-GF electrode for in situ bio-electroremediation of Cr(VI) contaminated groundwater.

Table 1
Parameters and data obtained from EIS analysis for all MFCs.

MFC type	Ohmic	R_{CT}	Capacitance	Warburg	error
MFC-A	4.7	2.68	$6.e^{-6}$	1.01	0.34
MFC-B	6.7	5.03	$1.85e^{-5}$	0.47	0.24
MFC—C	6.18	10.05	$1.47e^{-2}$	0.27	0.13

Maximum power output by MFCs was evaluated using polarization curves drawn by changing the external resistance. Cell potential data

was normalized with anode surface area to obtain power densities and current densities (Fig. 4c-d). Maximum extracted current density of MFC-A was 577 ± 0.1 mA/m^2 and it was 64 % and 135 % higher than the MFC-B (350.5 ± 0.3 mA/m^2) and MFC—C (245 ± 0.12 mA/m^2), respectively. Higher current densities can be attributed to the favorable electrochemical performance of NS/CNF-GF in MFC-A, which is due to low R_{ct}, more wettability and better electron transfer kinetics. Similar trend was observed for power generation, as MFC-A showed highest power density of 155 ± 0.3 mW/m^2 which was 83 % and 132 % higher than the MFC-B (84.8 ± 0.03 mW/m^2) and MFC—C (66 ± 0.02 mW/m^2), respectively.

High power density generated by MFC-A was ascribed to fast reduction of Cr(VI) in groundwater over numerous active sites created by thiourea etching. Yet MFC-B showed slightly better performance compared with MFC—C, which is only due to conductive CNFs on the GF. Bioenergy generated from MFCs can power the small biosensors and monitoring devices in wastewater treatment plants (Bataillou et al., 2024). Previous studies have demonstrated low power generation by Cr (VI) reducing MFCs, even under controlled environmental conditions like pH and electrolyte composition (Li and Zhou, 2018; Ma et al., 2022). For example, electrogenerated H_2O_2 from iron reducing bacteria reduced Cr(VI) and produced power density of 52 mW/m^2 at pH 2 (Liu et al., 2011). Tandukar et al. (2009) reported the higher power density of 55.5 mW/m^2 from the biocathode based MFC treating Cr(VI) in neutral aqueous solutions. Another study compared the PEM and bipolar membrane for Cr(VI) removing MFCs, which extracted power density of 47 and 150 mW/m^2 respectively. Thus, high power generation and improved electrokinetics in MFC-A signify the potential of self-standing cathode to remediate Cr(VI) from real groundwater.

3.4. Chromium remediation performance of MFC for treating real groundwater

Chromium (VI) remediation performance of all MFCs was studied using real groundwater to measure adsorption and reduction activity in open and closed circuits mode respectively. The reduction in Cr (VI) concentration during open circuit (OC) mode,can be attributed to the adsorption capacity of various cathodes (Fig. 5a). NS/CNF-GF showed highest adsorption (5.5 mg/L) of Cr(VI) among all electrodes, owing to large surface area and three-dimensional network of N, S co dopped CNFs. Notably, S atoms would have increased the wettability and hydrophilicity of cathodes (Fig. S1 and S3), and N doping can also increase interaction between CNFs and Cr (VI) for more absorption by electrostatic attraction, complexation and Van der Waals force (Chen et al., 2022). Remarkable adsorption capacity of PANI derived N dopped CNFs for hazardous wastes have been also reported (Khan et al., 2018). Relatively, low adsorption in CNF-GF was the result of fewer active sites in CNF network and absence of N, S atoms, while GF showed extremely low adsorption due to lack of CNFs. Adsorption of Cr (VI) is one of the most important mechanisms for water treatment in industrial setups (Chen et al., 2021b). Later, MFC circuits were closed by connecting both electrodes via external resistance (1000 Ω) for examining the Cr (VI) reduction in closed circuit modes. Unmodified cathode (GF) showed slightly high reduction (1.5 mg/L) than OC confirming the abiotic Cr(VI) reduction in actual groundwater under natural conditions. In contrast, modified cathodes showed substantially improved reduction of Cr(VI) in

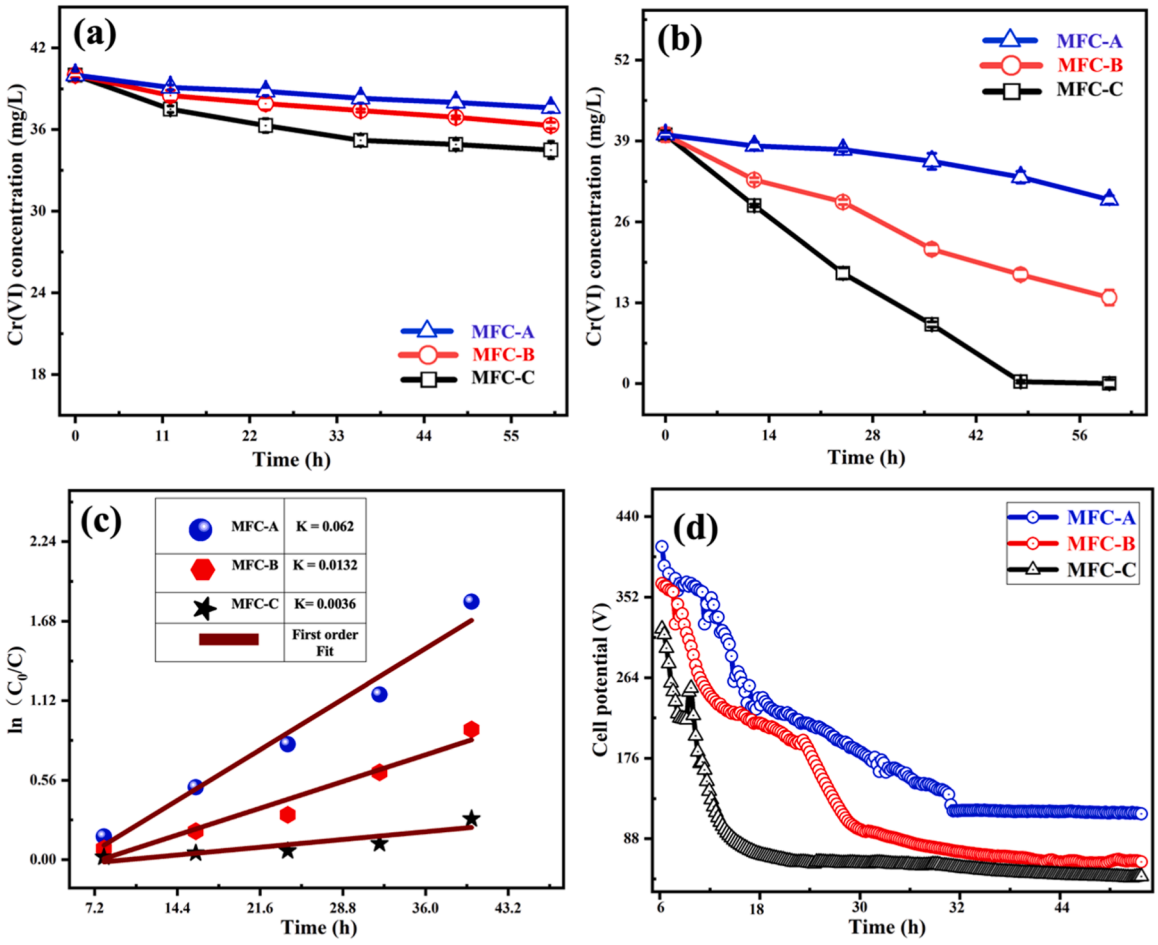

Fig. 5. Cr (VI) removal for all MFCs in OCP mode (a) closed circuit (b), Cr (VI) reduction kinetics and Pseudo order fitting (c), potential generated by MFCs inoculated with Cr (VI) contaminated groundwater.

groundwater. The Cr(VI) reduction efficiency was 100 %, 65% and 26% for MFC-A, MFC-B and MFC—C respectively after 48 h operation (Fig. 5b). The drastic improvement in Cr(VI) reduction by NS/NSF-GF validate the role of active sites on conductive CNFs for high adsorption and more electron transfer at pH of 7.4.

Low charge transfer resistance will facilitate the electron shuttling at cathode-electrolyte interface to indirectly promote the Cr(VI) reduction in groundwater. Electronegative S can facilitate the chemisorption of chromate ions on cathode to easily reduce Cr(VI). Reduction kinetic analysis and rate constants (k) provided in-depth details about MFC performance for treating real Cr(VI) contaminated groundwater under natural conditions. The rate constants (K) value for MFC-A (0.062/h) was higher compared to MFC-B (0.013/h) and MFC—C(0.0036/h), which indicate complete reduction of Cr(VI) requires additional time in control MFCs (Fig. 5c). Similarly, improved reduction kinetics were also evident from elevated reduction rate for MFC-A (0.83 mg/L/h), which was 73 and 273 times superior than that of MFC-B and MFC—C respectively (Fig. 5c). Enhanced bioelectroremediation of Cr(VI) contaminated groundwater on modified cathode can be correlated with increased electrogenic activity of anodic bacteria and generated potentials profiles in MFCs (Fig. 5d).

Favorable electrokinetics at cathode can also enhance the substrate consumption in anode to generate more electrons, which in turn accelerate the Cr(VI) reduction. The COD removal efficiency indirectly represent the electrogenic potential of anodic microbe, while number of electrons used for Cr(VI) reduction can be depicted from cathodic coulombic efficiencies ($C.E_{ca}$). So, COD removal efficiency and cathodic coulombic efficiency ($C.E_{ca}$) were also calculated to analyze detailed bio electroreduction of Cr(VI) in groundwater samples. Fig. 6a showing, COD removal efficiency for MFC-A (85± 2.1) was distinctly higher than that of MFC-B (70 ± 1.4) and MFC—C (57 ± 2.4). MFC-A exhibited the highest $C.E_{ca}$ (80 ± 1.3 %) compared with MFC-B (62 ± 1.7 %) and MFC—C(49 ± 2.6 %) respectively. A similar temporal trend was found between COD removal efficiency and $C.E_{ca}$ for MFC-A denoting the effectual performance of NS/NSF-GF for Cr(VI) reduction in groundwater (Fig. 6a). The pH measurement results showed that pH of catholyte in MFC-A had decreased from 7.4 to 7.06 ± 0.03, which was slightly more decrease in pH compared to MFC-B (7.18 ± 0.01)and MFC—C (7.24± 0.02) (Fig. S2). Reduction in pH for MFC-A can be referred to more protons and better conductivity of NS/CNF-GF cathode, which sustain the oxidizing power of $Cr_2O_7^{2-}$ and $HCrO_4$ to facilitate the Cr(VI) reduction under natural conditions. Previously, electrochemically generated protons have been employed to lower oxidation potential of Cr(VI) and subsequent reduction in flow-through cells at neutral pH of 8.0 (Wang et al., 2023). Long term performance and stability of modified electrodes was evaluated in Cr(VI) treating MFCs for another five 5 cycles. Current density profiles revealed that MFC-A performance was consistent throughout the operation (Fig. 6b), indicating the stability and reusability of NS/CNF-GF for large scale applications. However, gradual decrease in performance was observed for both MFC-B and

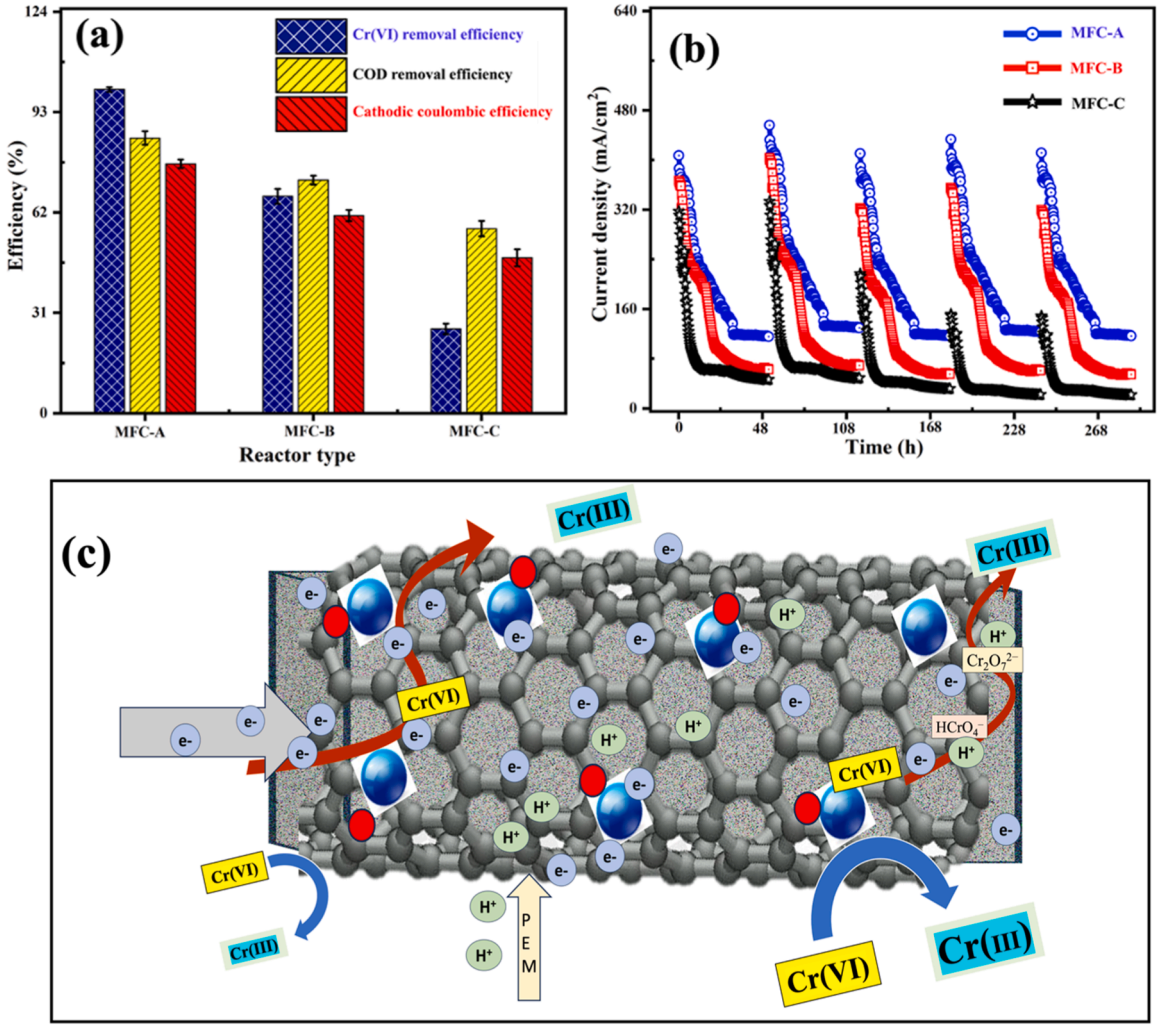

Fig. 6. (a) MFCs performance for Cr (VI) removal efficiency, COD removal and cathodic coulombic efficiency (b) reusability analysis of electrode and bioelectricity generation profiles, (c) Possible mechanism of enhanced Cr (VI) reduction on modified cathode.

MFC—C, probably due to, low wettability, blocked active sites and deteriorated conductive surface.

Herein, Cr(VI) removal efficiency is superior to previous reports, which have used similar setup, artificial wastewater, precious electrolytes, catalysts, biocathodes and have maintained acidic pH (Chen et al., 2022; Li and Zhou, 2018). Overall, current study provides sustainable electroremediation of Cr(VI) contaminated groundwater over self-standing cathode. Extremely stable and electroactive structure of cathode highlights its vast potential for treating multiple pollutants in groundwater and wastewater. Detailed investigations on pilot and large scale are suggested for using our cathode in field with high concentrations of Cr(VI). Moreover, influence of inhibitory anions on Cr(VI) removal in diverse pH range can be critical in remediation of Cr(VI) contaminated groundwater, which must be unveiled in future studies.

3.5. Possible mechanism for enhanced Cr(VI) reduction in groundwater

One possible pathway involves the direct reduction of Cr(VI) in vicinity of the cathode surface, which is a relatively slow reaction. Alternatively, the high conductivity of CNFs and the low R_{ct} of the NS/CNF-GF cathode collectively amplify the electron flux as confirmed by EIS and CV results. Simultaneously, S dopped sites enhance the cathode's wettability (Fig. S1) and foster the chemisorption of Cr(VI) species due to electrostatic attractions. The thiourea etching plays a vital role by creating N-containing active sites, electroactive turbostratic regions on CNFs and generating polarizing electrons. This synergistically enhances electrical conductivity and electron transfer to Cr(VI), expediting its transformation into less hazardous Cr(III). N dopped CNFs exhibit the capability to augment Cr(VI) adsorption by enhancing Van der Waals force, engaging in chemical complexation with cathode, and fostering electrostatic attractions. The implementation of a binder-free cathode proves instrumental in reducing the interfacial resistance between its surface and Cr(VI) contaminated groundwater. Protons, generated from the anaerobic oxidation of organic matter, travels to the cathode via the PEM (Fig. 6c), which help to sustain the oxidizing power of $Cr_2O_7^{2-}$ and $HCrO_4^-$, aligning with standard reduction potential by hydrogen ions. It consequently intensifies Cr(VI) reduction even in harsh and alkaline conditions (Ding et al., 2018; Wang et al., 2023). Therefore, the proposed method exhibits potential for practical field applications and in situ Cr(VI) remediation. Noteworthy advantages include minimal lab facilities requirements for electrode synthesis, heightened stability, and the ability to function under natural environmental conditions.

4. Conclusion

In this study, NS/CNF-GF was synthesized through in-situ polymerization method for the bio-electrochemical reduction of Cr(VI) in real groundwater. The utilization of this binder-free cathode ensured stability, minimizing additional costs, and streamlining electrode fabrication strategies. The enhanced electrochemical performance of the modified electrode was attributed to finely tuned active sites resulting from N, S doping, polarizing electron pairs, and improved electron transfer processes. NS/CNF-GF demonstrated complete reduction of 40 mg/L of Cr(VI) within 48 h, achieving a notable power density of 155± 0.3 mW/cm^2 at pH of 7.4. The accelerated reduction of Cr(VI) not only fostered electrogenic activity but also led to rapid COD removal in anode chamber. In-depth exploration of reduction kinetics, coupled with the attainment of the highest $C.E_{ca}$ of80 ± 1.3 % for MFC-A, substantiates that the primary charge consumption was attribute to Cr(VI) transformation in groundwater. Assessments of reusability and current generation profiles revealed the stability of the electrode, supporting its potential for practical applications in contaminated environments. Overall, the findings present novel avenues for in-situ remediation of Cr (VI) contaminated sites within natural systems, even under challenging environmental and hydrogeochemical conditions.

CRediT authorship contribution statement

Jafar Ali: Writing – review & editing, Writing – original draft, Methodology, Formal analysis, Conceptualization. **Changhong Zheng:** Software, Resources, Data curation. **Tao Lyu:** Writing – review & editing, Supervision. **Nurudeen Abiola Oladoja:** Writing – review & editing, Visualization, Data curation. **Ying Lu:** Writing – review & editing, Validation, Data curation. **Wengang An:** Writing – review & editing, Validation, Software. **Yuesuo Yang:** Writing – review & editing, Supervision, Project administration, Funding acquisition.

Declaration of competing interest

The authors declare that they have no known competing financial interests or personal relationships that could have appeared to influence the work reported in this paper.

Data availability

Data will be made available on request.

Acknowledgement

This work was supported by the Dingxin Post-doc Fellowship program to Dr. Jafar Ali at Jilin University, Changchun, China, and National Natural Science Foundation of China projects (Nos. 42277189, 42172284).

Supplementary materials

Supplementary material associated with this article can be found, in the online version, at doi:10.1016/j.watres.2024.121625.

References

Ali, J., Khan, A., Waseem, H., Djellabi, R., Anwar, P., Wang, L., Pan, G., 2021. Advances in the microbial fuel cell technology for the management of oxyanions in water. Progr. Prospect. Manag. Oxyanion Pollut. Aqua Syst. 219–236.

Ali, J., Wang, L., Waseem, H., Djellabi, R., Oladoja, N., Pan, G., 2020a. FeS@ rGO nanocomposites as electrocatalysts for enhanced chromium removal and clean energy generation by microbial fuel cell. Chem. Eng. J. 384, 123335.

Ali, J., Wang, L., Waseem, H., Sharif, H.M.A., Djellabi, R., Zhang, C., Pan, G., 2019. Bioelectrochemical recovery of silver from wastewater with sustainable power generation and its reuse for biofouling mitigation. J. Clean. Prod. 235, 1425–1437.

Ali, J., Wang, L., Waseem, H., Song, B., Djellabi, R., Pan, G., 2020b. Turning harmful algal biomass to electricity by microbial fuel cell: a sustainable approach for waste management. Environ. Pollut. 266, 115373.

Bataillou, G., Ondel, O., Haddour, N., 2024. 900-Days long term study of plant microbial fuel cells and complete application for powering wireless sensors. J. Power Sources 593, 233965.

Batayneh, A., 2012. Toxic (aluminum, beryllium, boron, chromium and zinc) in groundwater: health risk assessment. Int. J. Environ. Sci. Technol. 9, 153–162.

Chen, A., Liu, C., Yu, Y., Hu, Y., Lv, H., Zhang, Y., Shen, S., Zhang, J., 2014. A co-confined carbonization approach to aligned nitrogen-doped mesoporous carbon nanofibers and its application as an adsorbent. J. Hazard. Mater. 276, 192–199.

Chen, F., Guo, S., Wang, Y., Ma, L., Li, B., Song, Z., Huang, L., Zhang, W., 2022. Concurrent adsorption and reduction of chromium (VI) to chromium (III) using nitrogen-doped porous carbon adsorbent derived from loofah sponge. Front. Environ. Sci. Eng. 16, 1–11.

Chen, M., Le, T., Zhou, Y., Kang, F., Yang, Y., 2020. Thiourea-induced N/S dual-doped hierarchical porous carbon nanofibers for high-performance lithium-ion capacitors. ACS Appl. Energy Mater. 3 (2), 1653–1664.

Chen, W., Zhang, Y., Shi, W., Cui, Y., Zhang, Q., Shi, Y., Liang, Z., 2021a. Analysis of hydrogeochemical characteristics and origins of chromium contamination in groundwater at a site in Xinxiang City, Henan Province. Appl. Sci. 11 (24), 11683.

Chen, X., Dai, Y., Fan, J., Xu, X., Cao, X., 2021b. Application of iron-biochar composite in topsoil for simultaneous remediation of chromium-contaminated soil and groundwater: immobilization mechanism and long-term stability. J. Hazard. Mater. 405, 124226.

Dang, P., Wei, Y., Liu, D., Li, G., Lin, J., 2023. Recent advances in chromium-doped near-infrared luminescent materials: fundamentals, optimization strategies, and applications. Adv. Opt. Mater. 11 (3), 2201739.

Ding, J., Pu, L., Wang, Y., Wu, B., Yu, A., Zhang, X., Pan, B., Zhang, Q., Gao, G., 2018. Adsorption and reduction of Cr (VI) together with Cr (III) sequestration by

polyaniline confined in pores of polystyrene beads. Environ. Sci. Technol. 52 (21), 12602–12611.
Fan, M., Zhuang, X., Gao, Z., Lv, Z., Dong, W., Xin, F., Chen, Y., Jia, H., Wu, X., 2023. Electroactive microorganisms synthesizing iron sulfide nanoparticles for enhanced hexavalent chromium removal in microbial fuel cells. Sci. Total Environ. 889, 164311.
Fu, X.-Z., Wu, J., Cui, S., Wang, X.-M., Liu, H.-Q., He, R.-L., Yang, C., Deng, X., Tan, Z.-L., Li, W.-W., 2021. Self-regenerable bio-hybrid with biogenic ferrous sulfide nanoparticles for treating high-concentration chromium-containing wastewater. Water Res. 206, 117731.
Hidayat, A.R.P., Widyanto, A.R., Asranudin, A., Ediati, R., Sulistiono, D.O., Putro, H.S., Sugiarso, D., Prasetyoko, D., Purnomo, A.S., Bahruji, H., 2022. Recent development of double chamber microbial fuel cell for hexavalent chromium waste removal. J. Environ. Chem. Eng., 107505
Jalalabadi, T., Wu, J., Moghtaderi, B., Sharma, N., Allen, J., 2023. A new approach to turbostratic carbon production via thermal salt-assisted treatment of graphite. Fuel 348, 128489.
Jang, D., Lee, M.E., Choi, J., Cho, S.Y., Lee, S., 2022. Strategies for the production of PAN-Based carbon fibers with high tensile strength. Carbon N Y 186, 644–677.
Khan, N.A., An, H.J., Yoo, D.K., Jhung, S.H., 2018. Polyaniline-derived porous carbons: remarkable adsorbent for removal of various hazardous organics from both aqueous and non-aqueous media. J. Hazard. Mater. 360, 163–171.
Lai, Q., Zheng, J., Tang, Z., Bi, D., Zhao, J., Liang, Y., 2020. Optimal configuration of N-doped carbon defects in 2D turbostratic carbon nanomesh for advanced oxygen reduction electrocatalysis. Angew. Chem. 132 (29), 12097–12104.
Li, L., Tang, C., Zheng, Y., Xia, B., Zhou, X., Xu, H., Qiao, S.Z., 2020. Tailoring selectivity of electrochemical hydrogen peroxide generation by tunable pyrrolic-nitrogen-carbon. Adv. Energy Mater. 10 (21), 2000789.
Li, M., Zhou, S., 2018. α-Fe2O3/polyaniline nanocomposites as an effective catalyst for improving the electrochemical performance of microbial fuel cell. Chem. Eng. J. 339, 539–546.
Li, M., Zhou, S., 2019. Efficacy of Cu (II) as an electron-shuttle mediator for improved bioelectricity generation and Cr (VI) reduction in microbial fuel cells. Bioresour. Technol. 273, 122–129.
Liu, L., Yuan, Y., Li, F.-b., Feng, C.-h., 2011. In-situ Cr (VI) reduction with electrogenerated hydrogen peroxide driven by iron-reducing bacteria. Bioresour. Technol. 102 (3), 2468–2473.
Liu, Y., Li, G., Chen, Z., Peng, X., 2017. CNT-threaded N-doped porous carbon film as binder-free electrode for high-capacity supercapacitor and Li–S battery. J. Mater. Chem. A 5 (20), 9775–9784.
Luo, P., Xiao, Y., Yang, J., Zuo, C., Xiong, F., Tang, C., Liu, G., Zhang, W., Tang, W., Wang, S., 2022. Polyaniline nanoarrays/carbon cloth as binder-free and flexible cathode for magnesium ion batteries. Chem. Eng. J. 433, 133772.
Ma, L., Chen, N., Feng, C., Yao, Y., Wang, S., Wang, G., Su, Y., Zhang, Y., 2022. Enhanced Cr (VI) reduction in biocathode microbial electrolysis cell using Fenton-derived ferric sludge. Water Res. 212, 118144.
Mohapatra, D., Dhakal, G., Sayed, M.S., Subramanya, B., Shim, J.-J., Parida, S., 2019. Sulfur doping: unique strategy to improve the supercapacitive performance of carbon nano-onions. ACS Appl. Mater. Interfaces 11 (8), 8040–8050.
Prasad, S., Yadav, K.K., Kumar, S., Gupta, N., Cabral-Pinto, M.M., Rezania, S., Radwan, N., Alam, J., 2021. Chromium contamination and effect on environmental health and its remediation: a sustainable approaches. J. Environ. Manage. 285, 112174.
Qiu, W., Zhao, J., Song, X., Mao, Q., Ren, S., Hao, C., Xiao, Y., 2019. One-step activation synthesized hierarchical porous carbon spheres from resorcinol–thiourea–formaldehyde for electrochemical capacitors. Ind. Eng. Chem. Res. 59 (1), 226–235.
Shang, Y., Ding, Y., Zhang, P., Wang, M., Jia, Y., Xu, Y., Li, Y., Fan, K., Sun, L., 2022. Pyrrolic N or pyridinic N: the active center of N-doped carbon for CO2 reduction. Chin. J. Catal. 43 (9), 2405–2413.
Song, B., Li, J., Wang, Z., Ali, J., Wang, L., Zhang, Z., Liu, F., Glebov, E.M., Zhang, J., Zhuang, X., 2022. N-doped Fe nanoparticles anchored on 3D carbonized sugarcane anode for high power density and efficient chromium (VI) removal. J. Environ. Chem. Eng. 10 (6), 108751.
Song, B., Wang, Q., Ali, J., Wang, Z., Wang, L., Wang, J., Li, J., Glebov, E.M., Zhuang, X., 2023. Biochar-supported Fe3C nanoparticles with enhanced interfacial contact as high-performance binder-free anode material for microbial fuel cells. Chem. Eng. J. 474, 145678.
Tandukar, M., Huber, S.J., Onodera, T., Pavlostathis, S.G., 2009. Biological chromium (VI) reduction in the cathode of a microbial fuel cell. Environ. Sci. Technol. 43 (21), 8159–8165.
Walters, C.C., Kliewer, C.E., Awwiller, D.N., Rudnicki, M.D., Passey, Q.R., Lin, M.W., 2014. Influence of turbostratic carbon nanostructures on electrical conductivity in shales. Int. J. Coal. Geol. 122, 105–109.
Wang, G., Huang, L., Zhang, Y., 2008a. Cathodic reduction of hexavalent chromium [Cr (VI)] coupled with electricity generation in microbial fuel cells. Biotechnol. Lett. 30 (11), 1959–1966.
Wang, G., Huang, L., Zhang, Y., 2008b. Cathodic reduction of hexavalent chromium [Cr (VI)] coupled with electricity generation in microbial fuel cells. Biotechnol. Lett. 30, 1959–1966.
Wang, Y., Wang, C., Cheng, C., Wu, H., Liu, H., 2023. Chromium removal at neutral pHs via electrochemical Cr (VI) reduction and subsequent Cr (III) adsorption with MoS2 nanoflowers-modified graphite felt. J. Hazard. Mater. 455, 131582.
Wei, X., Zhang, W., Chen, L., Xia, X., Meng, Y., Liu, C., Lin, Q., Jiang, Y., Gao, S., 2022. Evaluation of graphitization and tensile property in microwave plasma treated carbon fiber. Diam. Relat. Mater. 126, 109094.
Wollbrink, A., Volgmann, K., Koch, J., Kanthasamy, K., Tegenkamp, C., Li, Y., Richter, H., Kämnitz, S., Steinbach, F., Feldhoff, A., 2016. Amorphous, turbostratic and crystalline carbon membranes with hydrogen selectivity. Carbon N Y 106, 93–105.
Wu, J., Zhang, Q., Li, M., Yan, J., Zhang, Y., Liu, J., Wu, Y., 2019. Nitrogen, sulfur-codoped micro–mesoporous carbon derived from boat-fruited sterculia seed for robust lithium–sulfur batteries. RSC Adv. 9 (28), 15715–15726.
Xafenias, N., Zhang, Y., Banks, C.J., 2013. Enhanced performance of hexavalent chromium reducing cathodes in the presence of Shewanella oneidensis MR-1 and lactate. Environ. Sci. Technol. 47 (9), 4512–4520.
Xu, L., Kijkla, P., Kumseranee, S., Punpruk, S., Gu, T., 2023. Corrosion-resistant" chromium steels for oil and gas pipelines can suffer from very severe pitting corrosion by a sulfate-reducing bacterium. J. Mater. Sci. Technol.
Xu, Y., Mo, Y., Tian, J., Wang, P., Yu, H., Yu, J., 2016. The synergistic effect of graphitic N and pyrrolic N for the enhanced photocatalytic performance of nitrogen-doped graphene/TiO2 nanocomposites. Appl. Catal. B 181, 810–817.
Xu, Y., Zhang, C., Zhou, M., Fu, Q., Zhao, C., Wu, M., Lei, Y., 2018. Highly nitrogen doped carbon nanofibers with superior rate capability and cyclability for potassium ion batteries. Nat. Commun. 9 (1), 1720.
Yu, Y., Ali, J., Yang, Y., Kuang, P., Zhang, W., Lu, Y., Li, Y., 2022. Synchronous Cr (VI) remediation and energy production using microbial fuel cell from a subsurface environment: a review. Energies 15 (6), 1989.
Zhang, B., Feng, C., Ni, J., Zhang, J., Huang, W., 2012. Simultaneous reduction of vanadium (V) and chromium (VI) with enhanced energy recovery based on microbial fuel cell technology. J. Power Sources 204, 34–39.
Zhang, M., Nautiyal, A., Du, H., Wei, Z., Zhang, X., Wang, R., 2021. Electropolymerization of polyaniline as high-performance binder free electrodes for flexible supercapacitor. Electrochim. Acta 376, 138037.
Zhang, W., Zhao, Y., Wang, X., Ma, X., Jin, L., Wang, H., Li, H., Yan, J., Pan, W., Chen, S., 2023a. Biocathode electrochemical activity and reduction characteristics of Cr (VI) system in microbial fuel cells. J. Chem. Technol. Biotechnol. 98 (6), 1478–1487.
Zhang, Y., Zhang, Q., Chen, W., Shi, W., Cui, Y., Chen, L., Shao, J., 2023b. Hydrogeochemical analysis and groundwater pollution source identification based on self-organizing map at a contaminated site. J. Hydrol. (Amst.) 616, 128839.
Zhou, C., Han, C., Min, X., Yang, T., 2022. Effect of different sulfur precursors on efficient chromium (VI) removal by ZSM-5 zeolite supporting sulfide nano zero-valent iron. Chem. Eng. J. 427, 131515.